Hindawi
Geofluids
Volume 2022, Article ID 7217560, 15 pages
https://doi.org/10.1155/2022/7217560

*Research Article*

# Pressure Transient Analysis for a Well Drilling into a Large-Size Cave in Fracture-Caved Carbonate Gas Reservoirs

**Jie Jin, Qingyu Li, and Detang Lu**

*Department of Modern Mechanics, University of Science and Technology of China, Hefei, Anhui 230027, China*

Correspondence should be addressed to Detang Lu; dtlu@ustc.edu.cn

Received 19 May 2022; Revised 28 June 2022; Accepted 5 July 2022; Published 4 August 2022

Academic Editor: Hao Wu



This paper studies the influence of large-size cave on pressure transient characteristics in fracture-caved carbonate gas reservoirs (FCCGR). With the rapid increase of energy demand, the exploration and development of unconventional oil and gas becomes more and more important. In recent years, many FCCGR have been discovered in western China and contribute significantly to Chinese gas reserves. However, with the presence of large-size cave, FCCGR have complex pore structures and strong heterogeneity. Traditional pressure transient analysis models cannot describe the gas flow accurately. This paper develops a novel pressure transient analysis model for FCCGR by coupling the fluctuating pressure and minor energy loss. Based on the solutions, the typical curves are plotted to analyze the pressure transient characteristics. It is found that the flow process can be subdivided into six stages, including the following: (I) wellbore storage, (II) first transition stage, (III) cave storage, (IV) second transition stage, (V) interporosity flow, and (VI) radial flow. The findings indicate that a concave is added, and the wellbore storage occurs earlier due to the existence of cave. Then, the influences of key parameters are studied. The pressure propagation coefficient and cave volume factor influence the stages I, II, III, and IV. When pressure propagation coefficient increases, the wellbore storage becomes larger and cave storage becomes smaller. The first concave moves to upper right. When cave volume factor increases, the wellbore storage occurs earlier and the curves move left in stage I. Interporosity flow factor and storage ratio influence the location and depth of the second concave. Finally, a field gas well is interpreted by using the proposed model, which verifies the reliability and correctness of the model. The findings of this study can help to better understand the influence of large-size cave on pressure transient characteristics. In addition, it can help engineers invert the cave volume, which is of great significance for the development in FCCGR.

## 1. Introduction

A large amount of crude oil and natural gas is stored in carbonate rock. There are many types of carbonate reservoirs, and fracture-caved carbonate gas reservoirs (FCCGR) are one of them. Recently, the exploration and development of FCCGR in China has shown a trend of rapid development, especially in Tarim, Ordos, and Sichuan basins [1]. FCCGR are formed by long-term geological process, such as sedimentation, tectonics, and karstification [2, 3]. The pore structures of FCCGR are very complex. FCCGR usually consist of high-permeability fractures, different-sized caves, and compact matrix [4, 5]. The fractures serve as the main flow path, whereas the caves and matrix serve primarily as storage areas [6, 7]. Therefore, they have complex fluid transport forms and high heterogeneity [8, 9]. FCCGR can generally be subdivided into two types. The most common one is small cave carbonate gas reservoirs, with the cave diameter ranging from millimeter to centimeter. Scholars use the triple medium model to investigate this type of gas reservoir. The other one is large-size cave carbonate gas reservoirs. The diameter of the cave ranges from meters and tens of meters [10]. This type of gas reservoirs is relatively rare. Such gas reservoirs can be seen in Tahe and Shunbei fields, northwest China. The buried depth of these FCCGR is very deep (6000 m~8300 m), and the temperature is very high (120°C~240°C) in Shunbei gas fields. Drilling engineers found that there would be drilling stem emptying and leak of drilling fluid during the drilling operation, which implies the well has drilled into a cave. Meanwhile, the seismic

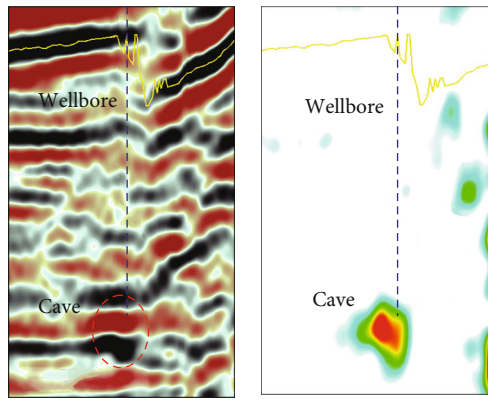


Figure 1: Geological information of the well drilling into a large-size cave. (a) Seismic section. (b) Residual wave impedance section.

section and residual wave impedance section also confirmed this situation. Figure 1 shows a typical FCCGR while the well has drilled into a large-size cave. The characteristics of gas reservoirs can be described by geological ways such as seismic response, logging, and drill core sampling. However, the above static ways are not accurate for dynamic production [11]. Well test has become an important dynamic way to describe gas reservoir characteristics. There are several types of well test, and the most common one is pressure transient analysis (PTA). Nowadays, PTA has turned into a significant way for analyzing the gas reservoirs characteristics [12]. The pressure transient behaviors in large-size cave carbonate gas reservoirs are different from the common FCCGR, especially when well has drilled into a cave. The gas in large-size cave does not obey Darcy law anymore, so the traditional dual medium model or triple medium model cannot describe the complex fluid dynamics in such gas reservoir accurately [13, 14]. As a result, developing a new PTA model for FCCGR when the well drilling into a cave is very essential.

The dual porosity medium model was proposed by Warren and Root [15]. On this basis, Abdassah and Ershaghi [16] established triple medium model, which contains matrix fractures and caves. Liu et al. [17] and Camacho-Velazquez et al. [18] viewed the cave like an extra matrix porosity component and presented several triple-continuum models. Then, Wu et al. [19] developed an analytical model for fractured-caved reservoirs. In their model, the caves directly connected to fractures are considered to be part of the fracture continuum. In recent years, many scholars began to investigate the influence of large-size cave for fracture-caved carbonate reservoirs. Zhang et al. [20] developed a well test model that the cave is considered as a higher permeability region. Liu and Wang [21] established a well test model for well drilling into a cave. They considered the cave as an equipotential body. Gao et al. [22] established a well test model including filled cave, matrix, and fractures. They considered the No-Darcy effect in filled cave. Du et al. [9] established a well test model for multivug carbonate reservoirs. Li et al. [23] established a well test model for vertical bead-on-string caves. Xing et al. [24] developed a PTA model for large-scale radial composite carbonate reservoirs. Their model can invert the number and position of large-size fractures and caves. As can be seen from the recent literatures, scholars consider the large-size cave as a separate pressure system. They think that the flow in fractures and matrix follows porous flow, while the flow in large-size cave follows free flow. Then, they couple the free flow and porous flow to develop well test model.

As mentioned above, there are many research achievements on fracture-cave carbonate reservoirs. However, in the existing literatures, the specific process of fluid entering the wellbore from large-size cave has not been studied. In these literatures, it is considered that the wellbore pressure is approximately equal to the cave pressure. But we think it is not accurate. Due to the strong compressibility of gas, there will be energy loss when gas enters the wellbore from large-size cave. In view of this, the equation between wellbore pressure and cave pressure is proposed in this paper. The results reveal that this change will significantly affect the shape of typical curves. The detailed discussion of the results is shown in Section 3.

The main objective of this paper is to establish a PTA model for a well drilling into a large-size cave in FCCGR. We propose a composite model consisting of the inner and the outer part. In the inner model, the equation between wellbore pressure and cave pressure is proposed. In the outer model, the dual porous medium equations are employed. The general sketch of the problem under study is shown in Figure 2.

The research results of this work can help better understand gas flow process in FCCGR. Through sensitivity analysis, the influence of large-size cave can be clearly identified. What is more, the developed model can be used for well test data analysis in FCCGR. It can help engineers invert important formation parameters, including wellbore storage constant, storage ratio, interporosity flow factor, and cave volume. Therefore, this work is crucial for understanding and developing FCCGR.

The organization of this paper is as follows: firstly, the physical model and corresponding mathematical model are developed in Section 2. Then, typical curves are plotted,

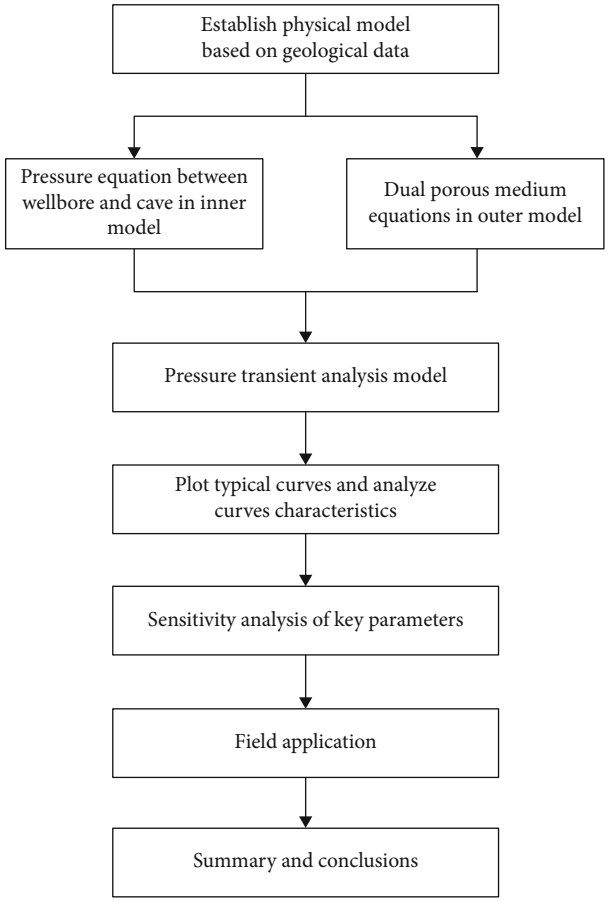


Figure 2: General sketch of the problem under study.

and two comparisons are made in Section 3. Next, the sensitivity analysis of key parameters is discussed in Section 4. Subsequently, the proposed model is applied on a field gas well in Section 5. Finally, summary and conclusions are presented in Section 6.

## 2. Physical and Mathematical Model

As mentioned above, the fluid transport form and pore structure of FCCGR are very complicated, which makes it difficult to simulate the gas flow process perfectly. In consideration of these problems, some assumptions are necessary to simplify the physical model.

*2.1. Assumptions and Physical Model.* The geological model of FCCGR can be converted into a physical model, as shown in Figure 3. Fractures and matrix are distributed in the formation. The wellbore is connected to a large-size cave. Meanwhile, some assumptions are made:

(1) The large-size cave is a cylinder, and the diameter of the cave is $d_{lc}$

(2) The formation is also a cylinder, and it is isotropic. The thickness of formation remains unchanged

To study the gas flow effectively, the model is subdivided into two parts: the inner model and the outer model, which is presented in Figure 4. The inner model includes wellbore and large-size cave. The outer model includes fractures and matrix. The height of wellbore in formation is $h_1$, and the height of large-size cave is $h_2$. In the outer model, the permeability of the matrix is much less than that of the fractures, so the gas directly entering the wellbore from the matrix can be ignored. In addition to the above settings, there are some other assumptions:

(3) The fluid in in the whole formation is only gas

(4) The well is located in the formation center and has a constant production $q_{sc}$. The initial pressure is consistent throughout the gas reservoir and equal to $p_0$

(5) In the outer model, the gas has a constant temperature and the Darcy's law is applicable

(6) Rock properties, such as permeability and porosity, remain unchanged

Subsequently, the mathematical model is established on the basis of the above assumptions. In the next section, the process of establishing the mathematical model will be shown.

*2.2. Mathematical Model.* Firstly, we study the inner model. In the procedure of gas entering the wellbore from the cave and then flowing in the wellbore, the continuity equation and the momentum equation need to be satisfied. In this flow procedure, only the vertical flow is considered. According to the work of Li et al. [25] and Wei et al. [26], the pressure in any part of the cave will immediately turn into balanced. Therefore, the cave can be regarded as an equipotential body. A large amount of gas is stored in large-size caves and wellbore, and a high-pressure gas storage space is formed. When the well opens, there will be fluctuating pressure caused by the compressibility of gas and pipe wall.

Take an infinitesimal element of wellbore to study, as shown in Figure 5. The length of this infinitesimal element is $\delta z$, and the cross-sectional area is $A$. First, the continuity equation and momentum equation are listed, as shown in Equations (1) and (2). In the momentum equation, the gravitational term of gas is ignored because the gravitational force of gas is too small.

$$\frac{\partial \rho}{\partial t} + \frac{\partial}{\partial z}(\rho v) = 0, \tag{1}$$

$$\frac{\partial}{\partial t}(\rho v) + \frac{\partial}{\partial z}\left(\rho v^2\right) = -\frac{\partial p}{\partial z} + \frac{\rho f v^2}{4 r_w}, \tag{2}$$

where $\rho$ is the gas density, $v$ is the velocity, $f$ is the friction coefficient, $r_w$ is the wellbore radius, $t$ is the time, and $z$ is the vertical length.

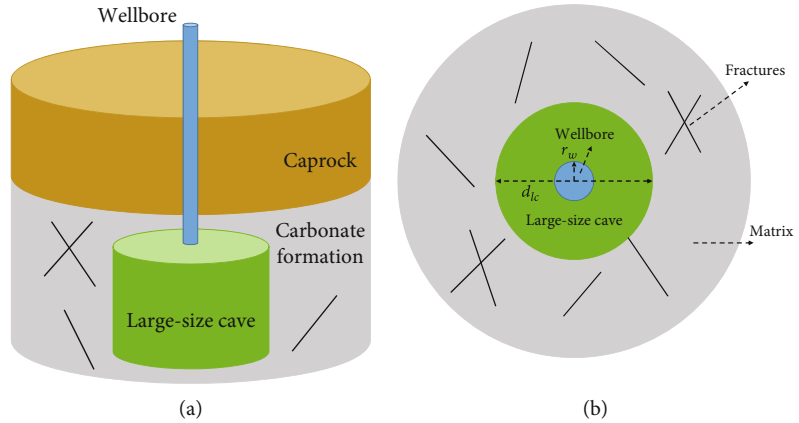


Figure 3: Physical model. (a) Front view of physical model. (b) Vertical view of physical model.

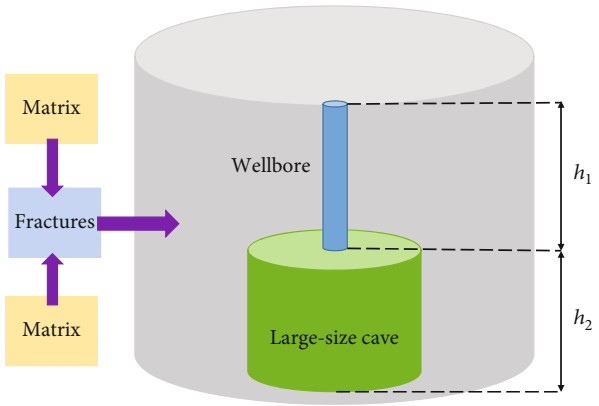


Figure 4: Schematic of inner model and outer model.

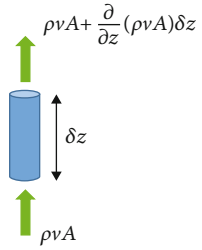


Figure 5: Schematic of infinitesimal element.

For the infinitesimal element, Equation (3) can be deduced from mass conservation.

$$\left[\rho Av + \frac{\partial(\rho Av)}{\partial z}\delta z\right] - \rho Av + \frac{\partial(\rho A)}{\partial t}\delta z = 0. \tag{3}$$

Equation (4) can be obtained from Equation (3):

$$\frac{\partial v}{\partial z} + \frac{1}{A}\frac{dA}{dt} + \frac{1}{\rho}\frac{d\rho}{dt} = 0. \tag{4}$$

Due to the high pressure, the wellbore will also deform. Its deformation is related to the tubing diameter, wall thickness, and elastic modulus of tubing material. Through formula derivation, the pressure propagation equation can be obtained as follows:

$$\frac{\partial p}{\partial t} + v\frac{\partial p}{\partial z} + \rho C^2\frac{\partial v}{\partial z} = 0. \tag{5}$$

From the above analysis, it can be found the pressure propagates as a wave in the z direction, and the wave velocity is $C$.

The gas velocity at the connection between wellbore and cave is as follows:

$$v_{wf} = \frac{1}{4}\frac{d_{lc}^2}{r_w^2}v_i \exp\left(-\frac{1}{4}\frac{\pi d_{lc}^2}{\rho C C_{lc}}t\right). \tag{6}$$

The derivation process of Equations (5) and (6) is shown in Appendix A.

The cross-sectional area of the cave is substantially larger than the cross-sectional area of the wellbore. Therefore, the connection area between the two is like a shrink tube. When the gas enters the wellbore from the cave, the flow velocity will increase rapidly, accompanied by the decrease of pressure. Meanwhile, part of the gas forms vortices near the tubing wall of wellbore, and these vortices will drain energy. The energy equation of gas from cave to wellbore is the following equation.

$$p_{lc} = p_{wf} + \frac{1}{2}\rho {v_{wf}}^2 + \rho g H_m, \tag{7}$$

where $p_{\mathrm{lc}}$ is the pressure of large-size cave, $p_{wf}$ is the pressure of bottom hole, and $H_m$ is the minor energy loss.

The formula of minor energy loss $H_m$ is as follows:

$$H_m = \frac{1}{2}\left(1 - \frac{A_w}{A_{lc}}\right)\frac{{v_{wf}}^2}{2g}, \tag{8}$$

where $A_w$ is the cross-sectional area of wellbore and $A_{lc}$ is the cross-sectional area of large-size cave.

Equation (9) is obtained by Equations (6)–(8).

$$p_{wf} = p_{lc} - \rho\left(\frac{3}{4} - \frac{r_w^2}{d_{lc}^2}\right)\left(\frac{1}{4}\frac{d_{lc}^2}{r_w^2}v_i\right)^2 \exp\left(-\frac{1}{2}\frac{\pi d_{lc}^2}{\rho C C_{lc}}t\right). \quad (9)$$

For the outer model, dual porous medium model is employed to characterize the gas transport. The dual porous medium model is composed of fractures and matrix. The fractures are the main flow channel while the matrix is the main storage space. The permeability of matrix is assumed to be 0. So there are two porosity and one permeability in the model. In the process of developing gas reservoirs, the gas can enter fractures from the matrix system and and then flows into the inner model [27].

For gas, introduce pseudopressure to substitute pressure [28].

$$m(p) = 2\int_{p_i}^{p} \frac{p}{\mu(p)\mathrm{z}(p)}dp, \quad (10)$$

where $p_i$ is a reference pressure and can be taken as any number.

The pressure variation equations are shown as follows:

$$\frac{k_f}{r}\frac{\partial}{\partial r}\left(r\frac{\partial m_f}{\partial r}\right) + \alpha k_m\left(m_m - m_f\right) = \mu\phi_f c_f \frac{\partial m_f}{\partial t}, \quad (11)$$

$$-\alpha k_m\left(m_m - m_f\right) = \mu\phi_m c_m \frac{\partial m_m}{\partial t}, \quad (12)$$

where $k$ is permeability, $\mu$ is viscosity, $c$ is compressibility coefficient, $\phi$ is the porosity, $\alpha$ is shape factor, subscript $f$ indicates the fractures system, and subscript $m$ indicates the matrix system.

When the gas approaches the wellbore, it will produce inertia-turbulence flow effect, which can create an additional pressure drop. Total skin factor is introduced to describe this pressure drop.

$$S_w = s_w + Dq_{\mathrm{sc}}, \quad (13)$$

where $S_w$ is the total skin factor, $s_w$ is real skin factor, and $q_{sc}$ is production rate of wellhead.

The bottom hole pressure can be calculated by the following equation:

$$m_{wf} = \left(m_f - S_w r\frac{\partial m_f}{\partial r}\right)\Big|_{r_w}. \quad (14)$$

The gas equation of state is as follows:

$$p = \frac{\rho RTz}{M}, \quad (15)$$

where $R$ is the universal constant of gas, $M$ is the gas molecular weight, and $z$ is the deviation factor of gas.

The production rate of gas under formation conditions is as follows:

$$q = q_{\mathrm{sc}}B_g = \frac{q_{\mathrm{sc}}p_{\mathrm{sc}}T}{pT_{\mathrm{sc}}}z. \quad (16)$$

The total production rate is composed of four parts: (1) wellbore storage (2), large-size cave storage (3), the gas from fractures to wellbore, and (4) The gas from fractures to large-size cave.

The formula is shown as follows.

$$-\frac{2q_{\mathrm{sc}}p_{\mathrm{sc}}T}{T_{\mathrm{sc}}\mu} = C_w\frac{\partial m_{wf}}{\partial t} + C_{\mathrm{lc}}\frac{\partial m_{\mathrm{lc}}}{\partial t} - 2\pi r_w h_1 \frac{k_f}{\mu}\frac{\partial m_f}{\partial r}\Big|_{r_w} - 2\pi r_{\mathrm{lc}} h_2 \frac{k_f}{\mu}\frac{\partial m_f}{\partial r}\Big|_{r_{\mathrm{lc}}}, \quad (17)$$

where $C_w$ is the storage constant of wellbore, $C_{\mathrm{lc}}$ is the storage constant of cave, and $r_{\mathrm{lc}}$ is the radius of cave.

According to the dimensionless definition in Table 1, Equations (9), (11), (12), (14), and (17) can be rewritten in dimensionless form, which are shown as follows.

$$\frac{\partial^2 m_{fD}}{\partial {r_D}^2} + \frac{1}{r_D}\frac{\partial m_{fD}}{\partial r_D} + \lambda\left(m_{mD} - m_{fD}\right) = \omega\frac{\partial m_{fD}}{\partial t_D}, \quad (18)$$

$$-\lambda\left(m_{mD} - m_{fD}\right) = (1-\omega)\frac{\partial m_{mD}}{\partial t_D}, \quad (19)$$

$$m_{wfD} = \left(m_{fD} - S_w r_D\frac{\partial m_{fD}}{\partial r_D}\right)\Big|_{r_D = 1}, \quad (20)$$

$$1 = C_{wD}\frac{\partial m_{wfD}}{\partial t_D} + C_{\mathrm{lcD}}\frac{\partial m_{\mathrm{lcD}}}{\partial t_D} - h_D\frac{\partial m_{fD}}{\partial r_D}\Big|_1 - (1-h_D)r_{\mathrm{lcD}}\frac{\partial m_{fD}}{\partial r_D}\Big|_{r_{\mathrm{lcD}}}, \quad (21)$$

$$m_{wfD} = m_{\mathrm{lcD}} + \varepsilon\exp\left(-\theta t\right). \quad (22)$$

In Equation (22), $\varepsilon$ and $\theta$ are the dimensionless parameters defined by this paper. $\varepsilon$ is called cave volume factor which is relative to the diameter and height of cave. $\theta$ is called pressure propagation coefficient. It is relative to the diameter of cave. Besides, $\theta$ is relative to the velocity of pressure wave and storage constant of large-size cave.

*2.3. Solution Strategy.* There are three outer boundary conditions of the proposed model, which are infinite formation, closed boundary, and constant pressure boundary. The equations are as follows.

$$\begin{cases} m_{fD}(r_D \longrightarrow \infty) = 0, \\ \dfrac{\partial m_{fD}}{\partial r_D}\Big|_{r_D = r_{eD}} = 0, \\ m_{fD}(r_D = r_{eD}) = 0. \end{cases} \quad (23)$$

Table 1: Dimensionless parameters.

| Parameters | Definitions |
|---|---|
| Dimensionless radius | $r_D = r/r_w$ |
| Dimensionless pseudopressure | $m_{jD} = \left(\pi k_f (h_1 + h_2) T_{sc}/(q_{sc} T p_{sc})\right)\left(m_i - m_j\right)$ |
| Dimensionless time | $t_D = \left(k_f/\left(\left(\phi_m c_m + \phi_f c_f\right)\mu_i {r_w}^2\right)\right)t$ |
| Dimensionless height | $h_D = h_1/(h_1 + h_2)$ |
| Storage ratio | $\omega = \phi_f c_f/\left(\phi_m c_m + \phi_f c_f\right)$ |
| Interporosity flow factor | $\lambda = \alpha\left(k_m/k_f\right){r_w}^2$ |
| Dimensionless wellbore storage constant | $C_{wD} = C_w/\left(2\pi\left(\phi_m c_m + \phi_f c_f\right)(h_1 + h_2) r_w^2\right)$ |
| Dimensionless large-size cave storage constant | $C_{lcD} = C_{lc}/\left(2\pi\left(\phi_m c_m + \phi_f c_f\right)(h_1 + h_2) r_w^2\right)$ |
| Pressure propagation coefficient | $\theta = 1/2\left(\pi {d_{lc}}^2 r_w^2\left(\phi_m c_m + \phi_f c_f\right)\mu_i z_i RT/\left(p_i M C C_{lc} k_f\right)\right)$ |
| Cave volume factor | $\varepsilon = 1/8\left(d_{lc}^4 {v_i}^2 \pi k_f (h_1 + h_2) T_{sc} p_i^2 M/\left(r_w^4 p_{sc} q_{sc} T^2 R z_i^2 \mu_i\right)\right)\left(3/4 - r_w^2/d_{lc}^2\right)$ |

The initial condition is as follows:

$$m_{fD}(r_D, t_D = 0) = m_{mD}(r_D, t_D = 0) = 0. \tag{24}$$

Laplace transform is employed to work out Equations (18)–(24). Subsequently, the dimensionless bottom hole pseudopressure can be gained in the Laplace domain after the Laplace transform.

$$\bar{m}_{wfD}(u) = F(u). \tag{25}$$

The particular derivation process is shown in the Appendix B. After that, the pseudopressure is transformed from Laplace domain to physics domain by Stehfest inversion [29].

$$m_{wfD}(t_D) = \frac{\ln 2}{t_D}\sum_{i=1}^{N} V_i \bar{m}_{wfD}(u), \tag{26}$$

where $V_i = (-1)^{N/2+i}\sum_{k=[i+1/2]}^{\min\ (i,N/2)} k^{N/2+1}(2k)!/(N/2-k)!k!(k-1)!(i-k)!(2k-i)!$.

## 3. Typical Curves and Discussion

Based on the solution, the typical curves of dimensionless bottom hole pseudopressures and pseudopressure derivative are plotted. Then, we analyze the characteristics of the curves in detail. In order to show how it differs from the triple medium model and verify the correctness, we compare our model with Wu's model [19] and Gao's model [22].

*3.1. Typical Curves.* The typical curves describe the transient transport characteristics graphically. Engineers can analyze the pressure transient changes and invert important formation parameters [30]. The double logarithmic curves are represented in Figure 6, which are in infinite formation conditions. The associated dimensionless parameters are given in the upper left corner of Figure 6.

Figure 6 shows the transient pseudopressure changes during the constant production of wellhead. They can be subdivided into six flow stages.

(1) Stage I represents the wellbore storage stage. During this stage, the wellhead production mainly comes from the gas originally stored in the wellbore. Both curves are straight lines with a slope of 1. Then, the skin effect appears, and the pseudopressure derivative curve is similar to a "hump"

(2) Stage II represents the transition stage between wellbore storage and cave storage. The original gas in the wellbore is gradually depleted, and the gas in large-size cave begins to flow into the wellbore. Due to the supplement of gas from cave, the dropping of pseudopressure slows down. As a result, the slope of the pseudopressure curve decreases. Meanwhile, there appears a concave in the derivative curve

(3) Stage III is the cave storage stage. The original gas in the wellbore is completely consumed, and the wellhead production mainly comes from the gas stored in the large-size cave storage. The slope of derivative curve is equals to 1. This stage is caused by the well drilling into a large-size cave. The shape of the curve can be used to judge whether the well drilling into a cave in FCCGR

(4) Stage IV represents the transition stage between cave storage stage and formation infiltrating stage. The gas in the fractures system enters the inner model. The wellhead production comes from the cave and fractures. During this stage, a phenomenon similar to skin effect emerges owing to the mutual effect between gas and wellbore cave. Hence, the

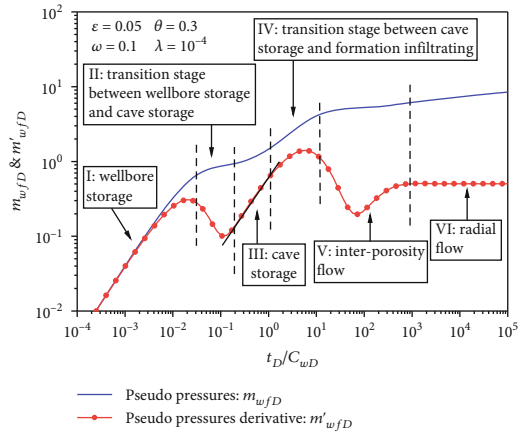


FIGURE 6: Typical curves of pseudopressure and pseudopressure derivative.

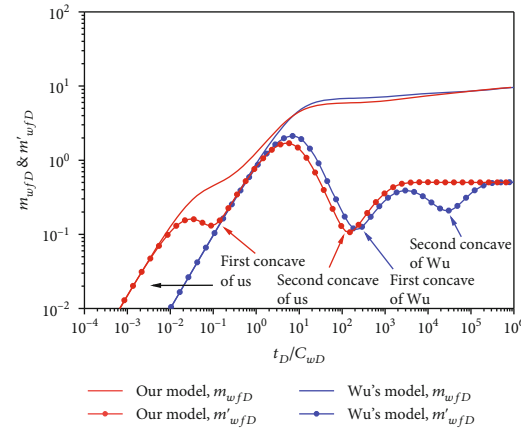


FIGURE 7: The typical curves comparison of Wu's model and our model.

pseudopressure derivative curve is similar to the end shape of stage I

(5) Stage V represents the interporosity flow stage between matrix and fractures. There is a differential pressure between matrix and fractures, which makes the gas in matrix flow into the fractures. Therefore, there is a concave in the derivative curve

(6) Stage VI represents the radial flow stage. The pseudopressure becomes dynamic balance, and the derivative curve gradually becomes a horizontal line

*3.2. Comparison with Wu's Model.* In order to better demonstrate our model's characteristics and show how it differs from the triple medium model, we make a comparison between our model and Wu's model.

Wu derived analytical solutions for bottom hole pressure in fracture-caved carbonate reservoirs. They established the model on the basis of triple medium model. In Wu's model, the fractures are main flow channel, while caves and matrix are main storage areas of fluid. Figure 7 shows the comparison results between Wu's model and our model.

There are obviously differences between the two models. Compared with Wu's model, the pseudopressure curve in our model moves to the left position in the wellbore storage stage. This is because the wellbore is connected to a large-size cave in our model, which is absent in Wu's model. In our model, when the well opens, there is fluctuating pressure caused by the compressibility of gas and pipe wall. This makes the wellbore pressure change quickly; hence, the wellbore storage stage occurs earlier.

There is a transition stage between the wellbore storage and large-size cave storage. Therefore, the first concave appears in our model. But there is no concave in Wu's model. The concave and the line segment with slope to 1 can be used to indicate the well drill into a cave.

In formation infiltrating stage, the second concave appears in derivative curve in our model. The concave represents the exchange flow between matrix and fractures. But there are two concaves in formation infiltrating stage in Wu's model. The first concave represents the exchange flow between caves and fractures. The second concave represents the exchange flow between matrix and fracture-cave system.

*3.3. Comparison with Gao's Model.* To validate our model, we compare our model with Gao's model.

Gao et al. established a PTA model for the well drilled into a large-size cave in fracture-caved carbonate reservoirs. In their model, the fluid flow in a filled cave was described by using the Barree-Conway model. Figure 8 shows the comparison results between Gao's model and our model.

The shapes of typical curves in the two models are similar. Besides, two concaves in our model and Gao' model appear in similar positions. The comparison results demonstrate our model is correct.

But there are some differences between the two models. As pointed by the green arrow, the wellbore storage stage occurs earlier in our model. This is because we considered the fluctuating pressure caused by gas and pip wall. Through the dimensionless parameters $\varepsilon$ and $\theta$, the volume of large-size cave connected to wellbore can be calculated. This makes the well test better interpret the information of formation.

## 4. Sensitivity Analysis

The typical curves have parameter sensitivity. Various parameters can change the shape of typical curves. In this section, we choose some key parameters to research their influences on typical curves.

*4.1. Influence of Outer Boundary Conditions.* When other parameters remain unchanged, by changing the outer boundary conditions, the typical curves of pseudopressure and pseudopressure derivative are plotted, as shown in Figure 9. There are three outer boundary conditions, which are closed boundary, infinite formation, and constant pressure boundary. From stages I to V, the curves of three outer boundary conditions are the same. But the difference occurs in stage VI. For closed boundary, the whole system has no energy supplement; hence, the pseudopressure persistently drops. This leads the pseudopressure curve and derivative

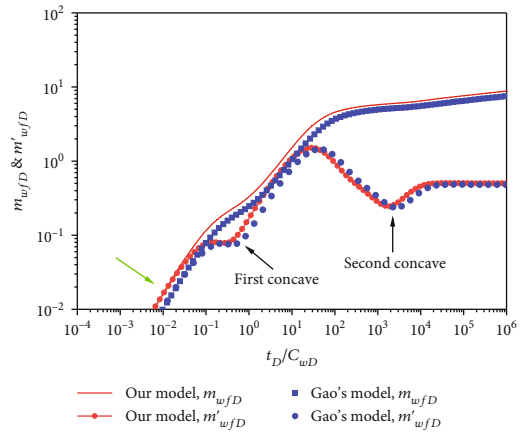


Figure 8: The typical curve comparison of Gao's model and our model.

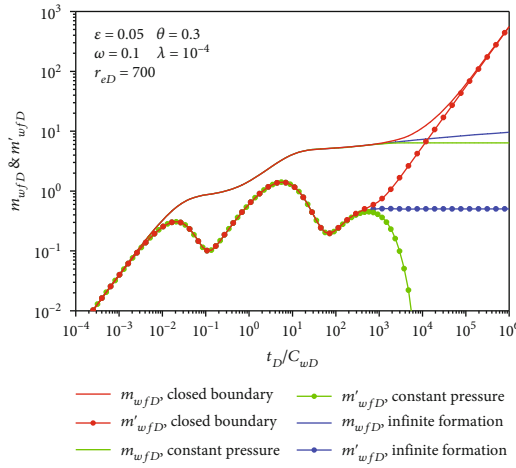


Figure 9: The influence of outer boundary conditions.

curve going upward. For constant boundary, the pseudopressure remains constant, which makes the pseudopressure curve becomes horizontal line and the derivative curve drops to 0. For infinite formation, the pseudopressure curve rises slowly and the derivative curve becomes horizontal line.

*4.2. Influence of Cave Volume Factor.* When outer boundary condition is infinite formation and other parameters remain unchanged, by changing cave volume factor, the typical curves are plotted, which is shown in Figure 10. It can be seen the cave volume factor influences the front part of the curves, including wellbore storage stage, first transition stage (stage II), large-size cave storage stage, and second transition stage (stage IV). When the cave volume factor increases, the pseudopressure curve moves up. This is because the pressure loss between the cave and wellbore increases with the larger $\varepsilon$. Hence, the bottom hole pressure becomes smaller, which reflected in the lager dimensionless pseudopressure. In stage I, when the cave volume factor increases, the pseudopressure curve moves to the left position. This shows that when the volume of cave becomes larger, the effect of fluctuation is greater, causing the wellbore storage to occur earlier. As

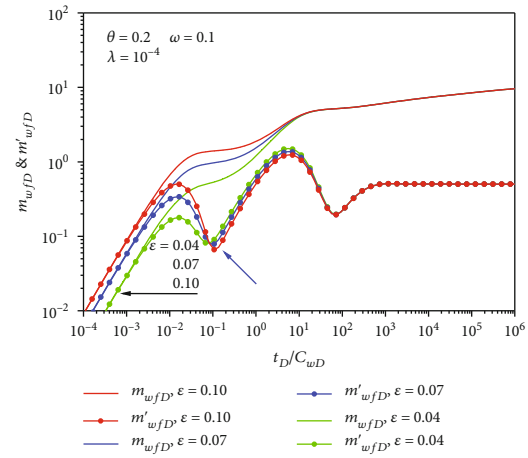


Figure 10: The influence of cave volume factor.

mentioned in Section 3, the concave that the blue arrow points to indicates the existence of cave. When the cave volume factor increases, the angle of concave becomes smaller, which can be used to judge the size of the cave. A small angle means a larger cave. In stages III and IV, cave volume factor slightly influences the derivative curve, which is reflected in the curve moving up a little with larger cave volume factor. In stages V and VI, the three pseudopressure curves coincide. At this time, the pseudopressure change comes from the formation infiltrating, and the influence of cave volume factor is negligible.

*4.3. Influence of Pressure Propagation Coefficient.* When outer boundary condition is infinite formation and other parameters remain unchanged, by changing pressure propagation coefficient, the typical curves are plotted, which is shown in Figure 11. It can be seen that pressure propagation coefficient also influences the front part of the curves. In stages V and VI, the influence of pressure propagation coefficient is negligible. The pressure propagation coefficient does not influence the initial period of wellbore storage stage. But the time of wellbore storage will be longer with larger pressure propagation coefficient. In stage II, the pseudopressure and pseudopressure derivative both increase with larger pressure propagation coefficient, and the first concave moves to upper right. This is because pressure propagation coefficient is related to the cave diameter. When it increases, the pressure loss between the wellbore and cave becomes larger, resulting in the rise of pseudopressure curve and derivative curve. Pressure propagation coefficient is also relative to large-size cave storage constant. Larger pressure propagation coefficient means smaller storage constant. Hence, the derivative curve becomes shorter and lower with larger pressure propagation coefficient in stage III. In stage IV, the influence of pressure propagation coefficient gradually decreases, and the three derivative curves begin to coincide.

*4.4. Influence of Storage Ratio.* When outer boundary condition is infinite formation and other parameters remain

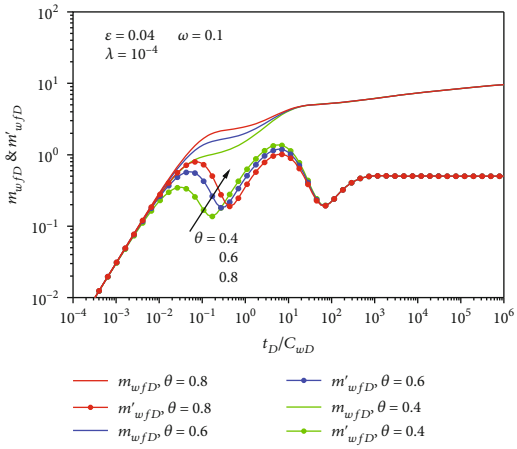


Figure 11: The influence of pressure propagation coefficient.

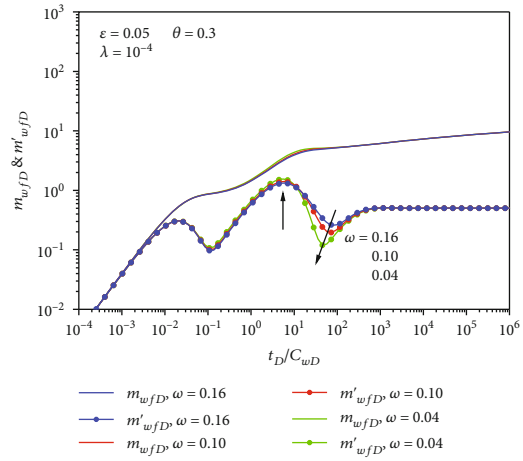


Figure 12: The influence of storage ratio.

unchanged, by changing storage ratio, the typical curves are plotted, which is shown in Figure 12. The $\omega$ is set to 0.16, 0.10, and 0.04. It can be seen $\omega$ influences the stage IV (transition stage) and stage V (exchange flow between matrix and fractures). In stage IV, when $\omega$ decreases, the derivative curve moves up slightly. In stage V, when $\omega$ decreases, the derivative curve moves down. As shown by the second arrow, the concave is deeper and moves to the left position with smaller $\omega$. These phenomena show the interporosity flow occurs earlier and more gas enters fractures with smaller $\omega$.

*4.5. Influence of Interporosity Flow Factor.* When outer boundary condition is infinite formation and other parameters remain unchanged, by changing interporosity flow factor, the typical curves are plotted. The interporosity flow factor is set to $10^{-4}$, $10^{-5}$, and $10^{-6}$. From Figure 13, we can find $\lambda$ mainly influences the stage V. When $\lambda$ becomes smaller, the concave moves to the right position, which means the interporosity flow occurred later. It is worth mentioning that the depth of the second concave ($\lambda = 10^{-5}$) and third concave ($\lambda = 10^{-6}$) is the same, but the depth of the first concave ($\lambda = 10^{-4}$) is shallow. When $\lambda = 10^{-4}$, the decrease of $\lambda$ can cause more gas enters fractures from matrix. But when $\lambda$ continues to decrease, it will not influence the amount of gas entering fractures.

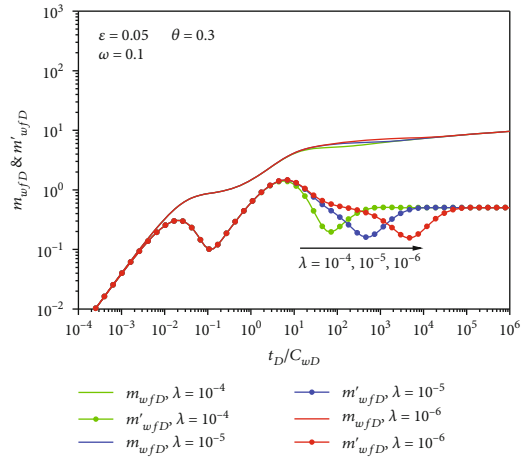


Figure 13: The influence of interporosity flow factor.

*4.6. Influence of Gas Reservoir Radius.* When outer boundary condition is closed boundary and other parameters remain unchanged, by changing gas reservoir radius, the typical curves are plotted. From the Figure 14, we can find the gas reservoir radius influences the transition stage (stage IV) and formation infiltrating stage (stages V and VI). When gas reservoir radius increases, the pseudopressure curve moves up. When $r_{ed} = 100$, the outer boundary will influence interporosity flow. When $r_{ed} = 500$, the outer boundary will not influence interporosity flow. Therefore, the increase of gas reservoir radius only makes the derivative curve in stage VI move up.

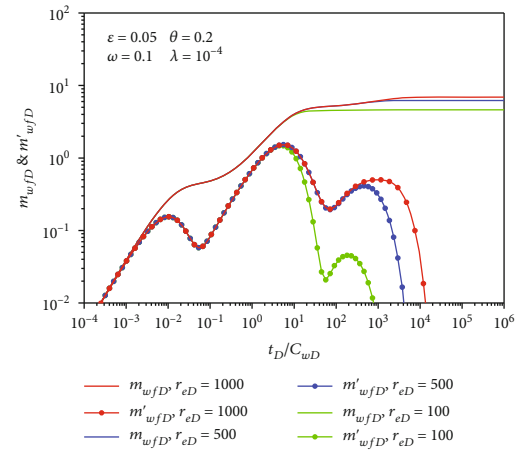


Figure 14: The influence of gas reservoir radius.

## 5. Field Example

PTA studies the changes of bottom hole pressure in the constant production of wellhead. According PTA, field engineers can get useful formation parameters [31]. To

Table 2: Properties of gas reservoir.

| Parameters | Values | Units |
|---|---|---|
| Wellbore radius | 0.1 | m |
| Porosity | 0.114 | Decimal |
| Composite compressibility of gas reservoir | 0.0062 | $MPa^{-1}$ |
| Wellbore height in formation | 10.5 | m |
| Gas reservoir temperature | 430.12 | K |
| Initial pressure | 80.38 | MPa |

further verify the proposed model and demonstrate its practical role in well test, we apply the model to a gas well from Shunbei.

As mentioned above, FCCGR are widely distributed in western China, with various sizes cave in formation. The gas well that we give an example locates in the second district of Shunbei, Xinjiang Province. The well depth is 6975 m, and the formation environment is high temperature and high pressure. Drilling engineers found a phenomena of drilling stem emptying and leak of drilling fluid during the drilling operation, which implies the well has drilled into a large-size cave. The seismic section and residual wave impedance section also proved this situation.

The well was in production for 11 days, with the constant production $q_{sc} = 61 \times 10^4\ m^3/d$. Then, the well was shut down. Engineers used highly accurate manometers to record the pressure build-up data for 151 hours. In the PTA, we should use the typical curves in proposed model to match the actual curves in pressure build-up data. Then, we can invert the formation parameters through matching results.

Table 2 displays the gas reservoir properties of the example well. Figure 15 represents the typical curve match between our model and field data. Figure 16 represents the pressure history match, and Figure 17 represents the dimensionless Horner match. It can be found that our model matches the field data well in the three figures. In view of the presented results, we can get conclusion that our model is very appropriate for this kind of gas well. The parameters of formation can be gained through the matching results, which are shown in Table 3. The diameter of the cave can be obtained by pressure propagation coefficient. Then, the height of the cave can be obtained by cave volume factor. Therefore, the cave volume can be calculated. The seismic data displays the cave volume is about 47000 $m^3$, and the interpretation result by our model displays the cave volume is 51202.05 $m^3$. The two results agree with each other.

In view of above statements, our model is recommended to interpret the FCCGR when well drilling into a large-size cave.

## 6. Summary and Conclusions

This paper represents a PTA model for a well drilling into a large-size cave in FCCGR. It is developed on the basis of filed geologic data in western China. Here are the main conclusions:

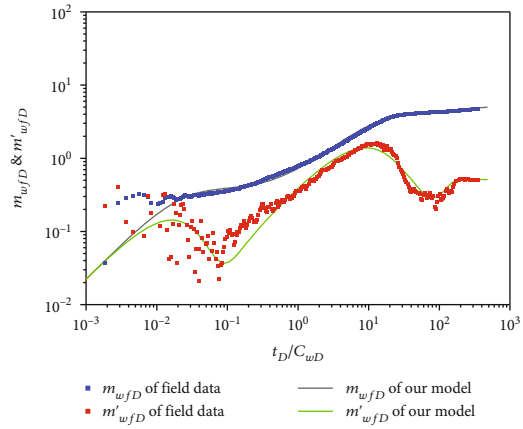


Figure 15: Typical curve match of the field data.

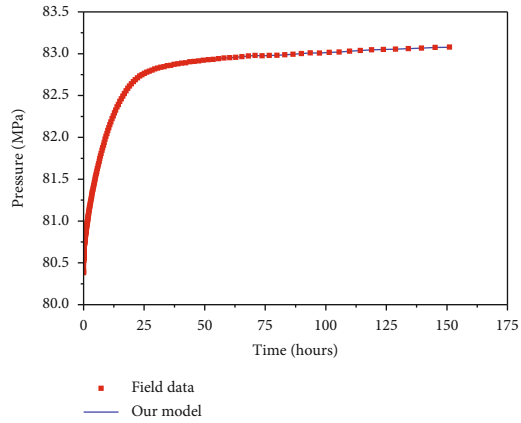


Figure 16: Pressure history match of the field data.

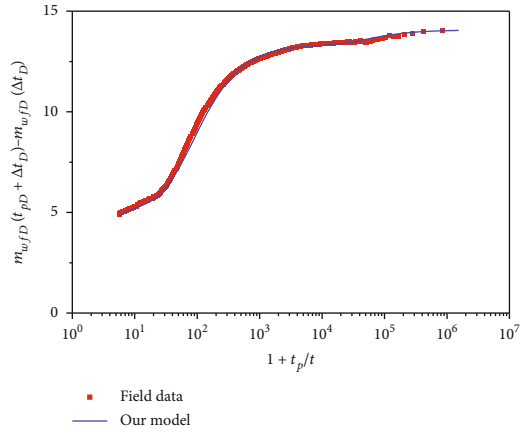


Figure 17: Dimensionless Horner match of the field data.

(1) The mathematical model is established with considering the minor energy loss and fluctuating pressure. The minor energy loss is formed at the connection area between the wellbore and cave. The fluctuating pressure is caused by the compressibility of gas and pipe wall. The solutions of the mathematical model are gained by Stehfest inversion. Subsequently, the typical curves are plotted

Table 3: Matching results.

| Parameters | Values | Units |
|---|---|---|
| Wellbore storage constant | 1.0248 | $m^3$/MPa |
| Total skin factor | 0.1896 | Decimal |
| Storage ratio | 0.1761 | Decimal |
| Interporosity flow factor | $7.162 \times 10^{-5}$ | Decimal |
| Cave volume factor | 0.0507 | Decimal |
| Pressure propagation coefficient | 0.2661 | Decimal |
| Cave volume | 51202.05 | $m^3$ |

(2) The typical curves can be subdivided into six stages. There are two concaves and two straight line segments in pseudopressure derivative curve. The first concave and the straight line segment of the cave storage can be used to indicate the well drill into a cave. The second concave indicates the exchange flow between matrix and fractures

(3) The cave volume factor $\varepsilon$ and the pressure propagation coefficient $\theta$ are key parameters that influence the front part of the curves. When $\varepsilon$ increases, the wellbore storage occurs earlier and the curves move left. Meanwhile, the pressure loss between the cave and wellbore increases, and the pseudopressure curve moves up. When $\theta$ increases, the cave storage becomes smaller and the wellbore storage becomes larger. The first concave moves to upper right

(4) To verify the proposed model and depict its characteristics, our model is compared with Wu's model and Gao's model. Then, a field gas well is interpreted by our model. The matching results fit well, and the interpretation parameters are reasonable. These results reveal that our model can be adapted to real gas reservoirs

In the mathematical model, the large-size cave is simplified as a cylinder. But in fact, cave is not a regular cylinder. This may cause some errors between the model and the actual situation.

In this work, we take into account fractures and matrix in the outer model. For some FCCGR, there are multiple large-size caves distributed in formation. Our model cannot be fit in this kind of gas reservoirs. Hence, we will develop new models for multiple caves in the future.

## Appendix

## A. Derivation of Pressure Wave Equation

When pressure increases, the relationship between wellbore radial deformation and pressure is as follows:

$$\frac{dD}{D} = \frac{D}{2eE_w} dp, \tag{A.1}$$

where $D$ is the tubing diameter, $D = 2r_w$, $e$ is the wall thickness of tubing, and $E_w$ is the elastic modulus of tubing material.

Equation (A.2) can be obtained from the area formula of tubing.

$$\frac{dA}{A} = 2\frac{dD}{D}. \tag{A.2}$$

Hence, Equation (A.3) can be obtained:

$$\frac{1}{A}\frac{dA}{dt} = \frac{D}{eE_w}\frac{dp}{dt}. \tag{A.3}$$

Convert the density term $\rho$ as a function of pressure, and combining Equations (A.3) and ((4)) can be turned into the following equation.

$$\frac{\partial v}{\partial z} + \left(\frac{1}{E_g} + \frac{D}{eE_w}\right)\frac{dp}{dt} = 0. \tag{A.4}$$

$C$ is defined as follows:

$$\frac{1}{C^2} = \rho\left(\frac{1}{E_g} + \frac{D}{eE_w}\right). \tag{A.5}$$

$C$ is the velocity of the pressure wave in the inner model, and $E_g$ is the elastic modulus of gas.

Equation (A.6) is obtained by Equation (A.4):

$$\frac{\partial p}{\partial t} + v\frac{\partial p}{\partial z} + \rho C^2\frac{\partial v}{\partial z} = 0. \tag{A.6}$$

It can be found the pressure propagates as a wave in the $z$ direction.

Equation (A.7) is obtained by Equations (1), (2), and (A.6).

$$\frac{dv}{dt} + \frac{1}{\rho C}\frac{dp}{dt} - \frac{4fv^2}{D} = 0. \tag{A.7}$$

When gas flows in the large-size cave, the velocity is very slow. The friction term is related to the quadratic power of velocity, so the friction term is extremely small and ignored.

The relationship between the storage constant of large-size cave and gas velocity is as follows:

$$C_{lc}\frac{dp}{dt} = \frac{1}{4}\pi {d_{lc}}^2 v, \tag{A.8}$$

where $C_{lc}$ is the storage constant of large-size cave.

Equation (A.7) can be can be converted to Equation (A.9).

$$\frac{dv}{dt} + \frac{1}{4\rho C}\frac{\pi d_{\mathrm{lc}}^2 v}{C_{\mathrm{lc}}} = 0. \tag{A.9}$$

The solution of Equation (A.9) is as follows:

$$v = v_i \exp\left(-\frac{1}{4}\frac{\pi d_{\mathrm{lc}}^2}{\rho C C_{\mathrm{lc}}} t\right), \tag{A.10}$$

where $v_i$ is the initial velocity, and it is related to wellhead production $q$.

The velocity at the connection between wellbore and cave is as follows:

$$v_{wf} = \frac{1}{4}\frac{d_{\mathrm{lc}}^2}{r_w^2} v_i \exp\left(-\frac{1}{4}\frac{\pi d_{\mathrm{lc}}^2}{\rho C C_{\mathrm{lc}}} t\right). \tag{A.11}$$

## B. Analytical Solutions of the Mathematical Model

The mathematical model established in Section 2 is as follows:

$$\frac{\partial^2 m_{fD}}{\partial {r_D}^2} + \frac{1}{r_D}\frac{\partial m_{fD}}{\partial r_D} + \lambda\left(m_{mD} - m_{fD}\right) = \omega\frac{\partial m_{fD}}{\partial t_D}, \tag{A.12}$$

$$-\lambda\left(m_{mD} - m_{fD}\right) = (1-\omega)\frac{\partial m_{mD}}{\partial t_D}, \tag{A.13}$$

$$m_{wfD} = \left(m_{fD} - S_w r_D \frac{\partial m_{fD}}{\partial r_D}\right)\Bigg|_{r_D = 1}, \tag{A.14}$$

$$1 = C_{wD}\frac{\partial m_{wfD}}{\partial t_D} + C_{lcD}\frac{\partial m_{lcD}}{\partial t_D} - h_D\frac{\partial m_{fD}}{\partial r_D}\Bigg|_1 - (1-h_D) r_{lcD}\frac{\partial m_{fD}}{\partial r_D}\Bigg|_{r_{lcD}}, \tag{A.15}$$

$$m_{wfD} = m_{lcD} + \varepsilon \exp\left(-\theta t\right). \tag{A.16}$$

The initial condition is as follows:

$$m_{fD}(r_D, t_D = 0) = m_{mD}(r_D, t_D = 0) = 0. \tag{A.17}$$

Laplace transform is as follows:

$$\bar{f}(u) = \int_0^\infty f(t) e^{-ut} dt. \tag{A.18}$$

Apply the Laplace transform to Equations (A.12)–(A.16):

$$\frac{\partial^2 \bar{m}_{fD}}{\partial {r_D}^2} + \frac{1}{r_D}\frac{\partial \bar{m}_{fD}}{\partial r_D} + \lambda\left(\bar{m}_{mD} - \bar{m}_{fD}\right) = \omega u \bar{m}_{fD}, \tag{A.19}$$

$$-\lambda\left(\bar{m}_{mD} - \bar{m}_{fD}\right) = (1-\omega) u \bar{m}_{mD}, \tag{A.20}$$

$$\bar{m}_{wfD} = \left(\bar{m}_{fD} - S_w r_D \frac{\partial \bar{m}_{fD}}{\partial r_D}\right)\Bigg|_{r_D = 1}, \tag{A.21}$$

$$\frac{1}{u} = C_{wD} u \bar{m}_{wfD} + C_{\mathrm{lc}D} u \bar{m}_{lcD} - h_D \frac{\partial \bar{m}_{fD}}{\partial r_D}\Bigg|_1 - (1-h_D) r_{\mathrm{lc}D} \frac{\partial \bar{m}_{fD}}{\partial r_D}\Bigg|_{r_{\mathrm{lc}D}}, \tag{A.22}$$

$$\bar{m}_{wfD} = \bar{m}_{\mathrm{lc}D} + \frac{\varepsilon}{\theta + u}. \tag{A.23}$$

From Equations (A.19) and (A.20), $\bar{m}_{fD}$ can be obtained:

$$\bar{m}_{fD} = AI_0\left(r_D\sqrt{uf(u)}\right) + BK_0\left(r_D\sqrt{uf(u)}\right), \tag{A.24}$$

where $f(u) = (\omega(1-\omega)u + \lambda)/((1-\omega)u + \lambda)$.

By introducing Equation (A.24) into Equations (A.21)–(A.23) and out boundary conditions, $\bar{m}_{wfD}$ can be obtained:

$$\bar{m}_{wfD} = WF_1 + NF_2. \tag{A.25}$$

(1) For the closed boundary

$$\frac{\partial \bar{m}_{fD}}{\partial r_D}\Bigg|_{r_D = r_{eD}} = 0, \tag{A.26}$$

where

$$
\begin{aligned}
N &= K_0\left(\sqrt{uf(u)}\right) + S_w\sqrt{uf(u)}K_1\left(\sqrt{uf(u)}\right),\\
W &= I_0\left(\sqrt{uf(u)}\right) - S_w\sqrt{uf(u)}I_1\left(\sqrt{uf(u)}\right),\\
F_1 &= \left(\frac{1}{u} + YC_{\mathrm{lc}D}u\right)[(C_{wD}uW + C_{\mathrm{lc}D}uW + E_2 + E_4)\\
&\quad + T_1(C_{wD}uN + C_{\mathrm{lc}D}uN + E_1 + E_3)]^{-1},\\
F_2 &= \left(\frac{T_1}{u} + T_1YC_{\mathrm{lc}D}u\right)[(C_{wD}uW + C_{\mathrm{lc}D}uW + E_2 + E_4)\\
&\quad + T_1(C_{wD}uN + C_{\mathrm{lc}D}uN + E_1 + E_3)]^{-1},\\
Y &= \frac{\varepsilon}{\theta + u},\\
E_1 &= h_D\sqrt{uf(u)}K_1\left(\sqrt{uf(u)}\right),\\
E_2 &= -h_D\sqrt{uf(u)}I_1\left(\sqrt{uf(u)}\right),\\
E_3 &= (1-h_D)r_{\mathrm{lc}D}\sqrt{uf(u)}K_1\left(\sqrt{uf(u)}r_{\mathrm{lc}D}\right),\\
E_4 &= -(1-h_D)r_{\mathrm{lc}D}\sqrt{uf(u)}I_1\left(\sqrt{uf(u)}r_{\mathrm{lc}D}\right),\\
T_1 &= \frac{I_1\left(\sqrt{uf(u)}r_{eD}\right)}{K_1\left(\sqrt{uf(u)}r_{eD}\right)}.
\end{aligned}
\tag{A.27}
$$

(2) For the constant pressure boundary

$$
\bar{m}_{fD}(r_D = r_{eD}) = 0, \tag{A.28}
$$

where

$$
\begin{aligned}
T_2 &= -\frac{I_0\left(\sqrt{uf(u)}r_{eD}\right)}{K_0\left(\sqrt{uf(u)}r_{eD}\right)},\\
F_1 &= \left(\frac{1}{u} + YC_{\mathrm{lc}D}u\right)[(C_{wD}uW + C_{\mathrm{lc}D}uW + E_2 + E_4)\\
&\quad + T_2(C_{wD}uN + C_{\mathrm{lc}D}uN + E_1 + E_3)]^{-1},\\
F_2 &= \left(\frac{T_2}{u} + T_2YC_{\mathrm{lc}D}u\right)[(C_{wD}uW + C_{\mathrm{lc}D}uW + E_2 + E_4)\\
&\quad + T_2(C_{wD}uN + C_{\mathrm{lc}D}uN + E_1 + E_3)]^{-1}.
\end{aligned}
\tag{A.29}
$$

$N, W, Y, E_1, E_2, E_3, E_4$ are the same form as in condition (1).

(3) For infinite formation

$$
\bar{m}_{fD}(r_D \longrightarrow \infty) = 0, \tag{A.30}
$$

where

$$
\begin{aligned}
F_1 &= 0,\\
F_2 &= \left(\frac{1}{u} + YC_{\mathrm{lc}D}u\right)[C_{wD}uN + C_{\mathrm{lc}D}uN + E_1 + E_3]^{-1}.
\end{aligned}
\tag{A.31}
$$

$N, Y, E_1, E_3$ are the same form as in condition (1).

## Nomenclature

*Alphabetic Letters*

$A$: Cross-sectional area, $m^2$
$B$: Formation volume factor, $m^3/m^3$
$C_j$: Storage constant, $Pa^{-1}$
$C$: Wave velocity, m/s
$D$: Tubing diameter, m
$E$: Elastic modulus, Pa
$H_m$: Minor energy loss, m
$M$: Gas molecular weight, kg/mol
$R$: Universal constant of gas, $8314\,m^2/s^2{\cdot}kmol{\cdot}K$
$S$: Skin factor, dimensionless
$T$: Temperature, K
$c$: Compressibility coefficient, $MPa^{-1}$
$d$: Diameter, m
$e$: Wall thickness of tubing, m
$f$: Friction coefficient, dimensionless
$g$: Gravity acceleration, $m/s^2$
$h$: Height, m
$k$: Permeability, $m^2$
$m$: Pseudopressure, $Pa^2/Pa{\cdot}s$
$p$: Pressure, Pa
$q$: Production rate, m/s
$r$: Radius, m
$t$: Time, s
$u$: Laplace operator, dimensionless
$v$: Velocity, m/s
$z$: Deviation factor of gas, dimensionless.

*Greek Letters*

$\alpha$: Shape factor, $m^{-2}$
$\varepsilon$: Cave volume factor, dimensionless
$\theta$: Pressure propagation coefficient, dimensionless
$\rho$: Density, $kg/m^3$
$\phi$: Porosity, dimensionless
$\mu$: Viscosity, Pa·s
$\omega$: Storage ratio, dimensionless
$\lambda$: Interporosity flow factor, dimensionless.

*Subscripts*

$D$: Dimensionless
$f$: Fractures
$g$: Gas
$i$: Initial state
$m$: Matrix

$p$: Shut-in well
$w$: Wellbore
$wf$: Bottom hole
sc: Standard state
lc: Large-size cave
$j$: Represent four systems, $j = f$, $m$, $w$, or lc.

*Superscript*

$'$: Derivative of time.

## Data Availability

The data used to support the conclusions of this study can be obtained from the corresponding author upon request.

## Conflicts of Interest

The authors state that the publishing of this paper does not include any conflicts of interest.

## Acknowledgments

The authors sincerely thank the National Science and Technology Major Project of China (Grant No. 2017ZX05009005-002) for the funding support.

## References

[1] A. Jia, H. Yan, J. Guo, D. He, L. Cheng, and C. Jia, "Development characteristics for different types of carbonate gas reservoirs," *Acta Petrolei Sinica*, vol. 34, no. 5, pp. 914–923, 2013.

[2] D. Zhu, Q. Liu, J. Zhang, Q. Ding, Z. He, and X. Zhang, "Types of fluid alteration and developing mechanism of deep marine carbonate reservoirs," *Geofluids*, vol. 2019, Article ID 3630915, 18 pages, 2019.

[3] V. Baques, E. Ukar, S. E. Laubach, S. R. Forstner, and A. Fall, "Fracture, dissolution, and cementation events in Ordovician carbonate reservoirs, Tarim Basin, NW China," *Geofluids*, vol. 2020, Article ID 9037429, 28 pages, 2020.

[4] Z. Huang, H. Xing, X. Zhou, and H. You, "Numerical study of vug effects on acid-rock reactive flow in carbonate reservoirs," *Advances in Geo-Energy Research*, vol. 4, no. 4, pp. 448–459, 2020.

[5] Q. Liu, B. Liang, J. Liu, W. Sun, and Y. Lei, "Imbibition oil recovery of single fracture-controlled matrix unit: model construction and numerical simulation," *Capillarity*, vol. 5, no. 2, pp. 32–40, 2022.

[6] Z. Q. Huang, J. Yao, and Y. Y. Wang, "An efficient numerical model for immiscible two-phase flow in fractured karst reservoirs," *Communications in Computational Physics*, vol. 13, no. 2, pp. 540–558, 2013.

[7] Q. Yu, Q. Wang, P. Liu et al., "Theoretical study and application of rate transient analysis on complex fractured-caved carbonate reservoirs," *Geofluids*, vol. 2021, Article ID 6611957, 15 pages, 2021.

[8] J.-C. Guo, R.-S. Nie, and Y.-L. Jia, "Dual permeability flow behavior for modeling horizontal well production in fractured-vuggy carbonate reservoirs," *Journal of Hydrology*, vol. 464-465, pp. 281–293, 2012.

[9] X. Du, Q. Li, Z. Lu et al., "Pressure transient analysis for multi-vug composite fractured vuggy carbonate reservoirs," *Journal of Petroleum Science and Engineering*, vol. 193, article 107389, 2020.

[10] C. Peng, X. Wang, L. Hong, Y. Huang, and Z. Hao, "A pressure-transient model for a fractured-vuggy carbonate reservoir with large-scale cave," *Geosystem Engineering*, vol. 19, no. 2, pp. 1–8, 2016.

[11] Y.-Z. Wan, Y.-W. Liu, F.-F. Chen, N.-Y. Wu, and G.-W. Hu, "Numerical well test model for caved carbonate reservoirs and its application in Tarim Basin, China," *Journal of Petroleum Science and Engineering*, vol. 161, pp. 611–624, 2018.

[12] Y. L. Zhao, L. H. Zhang, J. X. Luo, and B. N. Zhang, "Performance of fractured horizontal well with stimulated reservoir volume in unconventional gas reservoir," *Journal of Hydrology*, vol. 512, pp. 447–456, 2014.

[13] X. Yan, Z. Huang, J. Yao et al., "Numerical simulation of hydro-mechanical coupling in fractured vuggy porous media using the equivalent continuum model and embedded discrete fracture model," *Advances in Water Resources*, vol. 126, pp. 137–154, 2019.

[14] L. Wang, X. Wang, E. Luo, and J. Wang, "Analytical modeling of flow behavior for wormholes in naturally fractured–vuggy porous media," *Transport in Porous Media*, vol. 105, no. 3, article 383, pp. 539–558, 2014.

[15] J. E. Warren and P. J. Root, "The behavior of naturally fractured reservoirs," *Society of Petroleum Engineers Journal*, vol. 3, no. 3, pp. 245–255, 1963.

[16] D. Abdassah and I. Ershaghi, "Triple-porosity systems for representing naturally fractured reservoirs," *SPE Formation Evaluation*, vol. 1, no. 2, pp. 113–127, 1986.

[17] J. C. Liu, G. S. Bodvarsson, and Y. S. Wu, "Analysis of flow behavior in fractured lithophysal reservoirs," *Journal of Contaminant Hydrology*, vol. 62-3, pp. 189–211, 2003.

[18] R. Camacho-Velazquez, M. Vasquez-Cruz, R. Castrejon-Aivar, and V. Arana-Ortiz, "Pressure-transient and decline-curve behavior in naturally fractured vuggy carbonate reservoirs," *SPE Reservoir Evaluation & Engineering*, vol. 8, no. 4, pp. 266–266, 2005.

[19] Y.-S. Wu, C. A. Ehlig-Economides, G. Qin et al., "A triple-continuum pressure-transient model for a naturally fractured vuggy reservoir," in *SPE Annual Technical Conference and Exhibition*, Anaheim, California, U.S.A, 2007.

[20] F. Zhang, F. Chen, J. Peng, Y. Jia, and J. Yang, "A well test model for wells drilled in big-size cavity of naturally fractured vuggy carbonate reservoirs," *Acta Petrolei Sinica*, vol. 30, no. 6, pp. 912–915, 2009.

[21] H. Liu and X. Wang, "Pressure response characteristics in large scale cavity type reservoir," *Journal of Southwest Petroleum University*, vol. 34, no. 4, pp. 94–99, 2012.

[22] B. Gao, Z.-Q. Huang, J. Yao, X.-R. Lv, and Y.-S. Wu, "Pressure transient analysis of a well penetrating a filled cavity in naturally fractured carbonate reservoirs," *Journal of Petroleum Science and Engineering*, vol. 145, pp. 392–403, 2016.

[23] Q. Li, X. Du, Q. Tang, Y. Xu, P. Li, and D. Lu, "A novel well test model for fractured vuggy carbonate reservoirs with the vertical bead-on-a-string structure," *Journal of Petroleum Science and Engineering*, vol. 196, article 107938, 2021.

[24] C. Xing, H. Yin, H. Yuan, J. Fu, and G. Xu, "Pressure transient analysis for fracture-cavity carbonate reservoirs with large-scale fractures-caves in series connection," *Journal of Energy*

*Resources Technology-Transactions of the Asme*, vol. 144, no. 5, pp. 1–17, 2022.

[25] Y. Li, Q. Yu, C. Jia, P. Liu, Q. Wang, and D. Wang, "Rate transient analysis for coupling Darcy flow and free flow in bead-string fracture-caved carbonate reservoirs," *Journal of Petroleum Science and Engineering*, vol. 195, p. 107809, 2020.

[26] C. Wei, S. Cheng, J. Song et al., "Pressure transient analysis for wells drilled into vertical beads-on-string caves in fracture-caved carbonate reservoirs: field cases in Shunbei Oilfield," *Journal of Petroleum Science and Engineering*, vol. 208, article 109280, 2022.

[27] T. Zhang, Z. Li, C. D. Adenutsi, and F. Lai, "A new model for calculating permeability of natural fractures in dual-porosity reservoir," *Advances in Geo-Energy Research*, vol. 1, no. 2, pp. 86–92, 2017.

[28] R. Al-Hussainy, H. Jr, and P. B. Crawford, "The flow of real gases through porous media," *Journal of Petroleum Technology*, vol. 18, no. 5, pp. 624–636, 1966.

[29] H. Stehfest, "Algorithm 368: numerical inversion of Laplace transforms D5," *Communications of the ACM*, vol. 13, no. 1, pp. 47–49, 1970.

[30] M. Dejam, H. Hassanzadeh, and Z. Chen, "Semi-analytical solution for pressure transient analysis of a hydraulically fractured vertical well in a bounded dual-porosity reservoir," *Journal of Hydrology*, vol. 565, article S0022169418306164, pp. 289–301, 2018.

[31] X. Du, Q. Li, P. Li, Y. Xian, Y. Zheng, and D. Lu, "A novel pressure and rate transient analysis model for fracture-caved carbonate reservoirs," *Journal of Petroleum Science and Engineering*, vol. 208, article S0920410521012456, p. 109609, 2022.